Computational and Experimental Research in Materials and Renewable Energy (CERiMRE)
Volume 8, Issue 1, page 1-18
eISSN : 2747-173X

Submitted : April 24, 2025
Accepted : May 19, 2025
Online : May 31, 2025
DOI : 10.19184/cerimre.v8i1.53687

Fluid Dynamics Exploration in Molten Salt Reactors: A Comprehensive Study of Draining Tank Using the Moving Particle Semi-Implicit Method

Yacobus Yulianto[1], Asril Pramutadi Andi Mustari[2,a], Muh. Rizqie Arbie[2]

[1]Department of Physics, Halu Oleo University, Kendari, Indonesia

[2]Department of Physics, Bandung Institute of Technology, Bandung, Indonesia

[a]pramutadi@itb.ac.id

Abstract. *Molten Salt Reactors (MSRs) represent a promising advancement in nuclear energy technology through the use of liquid fuels, offering inherent safety features and efficient thermal conversion. A critical safety mechanism in MSRs is the drain tank system, designed to passively remove molten salt fuel during emergency shutdowns. This study presents a comprehensive hydrodynamic analysis of the draining process in such tanks using the Moving Particle Semi-Implicit (MPS) method, a mesh-free Lagrangian computational fluid dynamics technique well-suited for simulating free-surface flows. The investigation focused on key parameters including discharge velocity, pressure distribution, discharge rate, discharge coefficient, and Reynolds number for three fluids: light water, FLiBe (LiF-BeF_2), and FLiNaK (LiF-NaF-KF). Simulations were performed under isothermal conditions, neglecting heat transfer to isolate pure fluid dynamic behavior. Results reveal a consistent discharge pattern across all fluids, characterized by an initial rapid flow phase followed by gradual stabilization. FLiBe and FLiNaK, due to their higher densities and viscosities, exhibited slightly greater initial velocities and pressures than light water, yet all fluids demonstrated similar discharge rates and coefficients over time. The Reynolds number analysis confirmed turbulent flow regimes throughout the drainage process for each fluid. Despite differences in physical properties, the overall draining behavior and temporal trends in velocity and pressure were remarkably similar. These findings validate the use of MPS in analyzing transient liquid dynamics in MSR safety systems and provide valuable insights into reactor design optimization. Future work incorporating thermal effects could further enhance understanding of coupled thermofluid behavior, supporting the development of MSRs as a reliable and sustainable energy solution.*

Keywords: drainage, FLiBe, FLiNaK, liquid, MPS, MSR

Introduction

Incidents at Three Mile Island, Chernobyl, and Fukushima Daiichi have caused a significant increase in the global understanding of nuclear reactor safety. These events, each with unique challenges, have played a pivotal role in shaping and reinforcing safety protocols within the nuclear industry. The nuclear industry has implemented several safety measures in place in response to these severe accidents. Enhanced safety systems are now integral to nuclear power plants, allowing prompt detection and response to abnormal conditions. Reactor designs have been improved to incorporate inherent safety features that passively mitigate accidents and reduce the reliance on active safety systems.

Molten Salt Reactors (MSRs) represent a promising and innovative approach for nuclear energy generation. These reactors utilize liquid fuel composed of a mixture of fissile materials and fluoride-based salt coolant, offering several advantages over traditional solid-fueled reactors. A Molten Salt Reactor (MSR) is an advanced type of nuclear reactor that utilizes a liquid mixture

Computational and Experimental Research in Materials and Renewable Energy (CERiMRE)
Volume 8, Issue 1, page 1-18
eISSN : 2747-173X

Submitted : April 24, 2025
Accepted : May 19, 2025
Online : May 31, 2025
DOI : 10.19184/cerimre.v8i1.53687

of salts to serve simultaneously as the fuel and the coolant. The essential characteristic of MSR is the use of liquid fuel instead of solid fuel rods. These MSRs provide advantages; however, there are also technological challenges. For example, the corrosive nature of molten salts must be addressed, and suitable materials must be developed for the components of reactors as performed by these researchers [1], [2], [3], [4], [5], [6], [7]. To address these issues and assess the likelihood of molten salt reactors being widely used in the future, ongoing research and development is being performed.

The concept of a drain tank is one of the most important safety elements of MSRs. Owing to its ability to control reactor heat and maintain coolant flow even in the event of an active power outage, this component is essential for guaranteeing the passive and inherent safety of MSRs. The complex operation of drain tank in a molten salt reactor was explored in this study. To simulate the model, all calculations were performed by using the MPS method. This method employs a mesh-less computational fluid dynamics (CFD) approach to model incompressible fluid flows, representing the fluid as discrete particles that move and interact according to governing physical principles. This method was first introduced by Koshizuka and Oka [8], [9]. It is very suitable for modeling free-surface flows, particularly in fluid-structure interaction situations, e.g. solid-liquid flows [10], [11] and fluid-structure interactions [12], [13]. Some researchers had proven this method to investigate some phenomena in nuclear reactor, e.g. relocation [12], [14], [15] and eutectic [16], [17].

In this study, the volume of the liquid inside the tank, discharge velocity, pressure distribution, discharge rate, discharge coefficient, and Reynolds number were analyzed to study the behavior of the liquid inside the tank during the discharge process. By meticulously simulating various scenarios, including reactor transients and emergency shutdowns, the performance of the drain tank in mitigating potential accidents and maintaining the integrity of the reactor can be evaluated. The simulation was performed using the source code adopted from these references [15], [18], [19]. The dependability and precision of this source code have been examined and verified using other phenomena [20], [21], [22]. The obtained results of this study were compared to those of Rechiman et al. [23]. The MSR fuel liquids, FLiBe and FLiNaK, are utilized in addition to light water. Previous researchers had performed a number of investigations on MSR using FLiBe [2], [24], [25] and FLiNaK [1], [2], [6], [25].

This study presents an alternative approach for analyzing the hydrodynamic properties of a drainage tank in a nuclear reactor safety system. This was achieved by developing a simplified model using the Moving Particle Semi-Implicit framework. The source code had been adopted from these references [15], [19]. By comprehending the behavior of the drain tank under various circumstances, the security and dependability of nuclear energy can be enhanced by ensuring the robustness and safety of this cutting-edge technology. The results of this research provide information that can contribute to the advancement of MSR as a clean-sustainable energy source in the future.

Computational and Experimental Research in Materials and Renewable Energy (CERiMRE)
Volume 8, Issue 1, page 1-18
eISSN : 2747-173X

Submitted : April 24, 2025
Accepted : May 19, 2025
Online : May 31, 2025
DOI : 10.19184/cerimre.v8i1.53687

Mathematical Model, Numerical Method, and Simulation

Mathematical Model

By treating the liquid as a volumetric particle, the MPS method applies the Lagrangian approach. Following [8], [9], [26], the weight function given in the equation governs the interaction between particles as

$$w(|\vec{r}|) = \begin{cases} \frac{r_e}{r} - 1 & 0 \le r < r_e \\ 0 & r_e \le r \end{cases} \quad (1)$$

where r_e is the cut-off radius of interaction and r is the distance between the two closest particles. This indicates that only particles inside the radius will have an impact on the referred particle, or i-particle, which is known as the effective radius. Neighboring particles, or j-particles, are defined as particles inside the effective radius. A schematic depiction of a referred particle interacting with a nearby particle is presented in **Figure 1**.

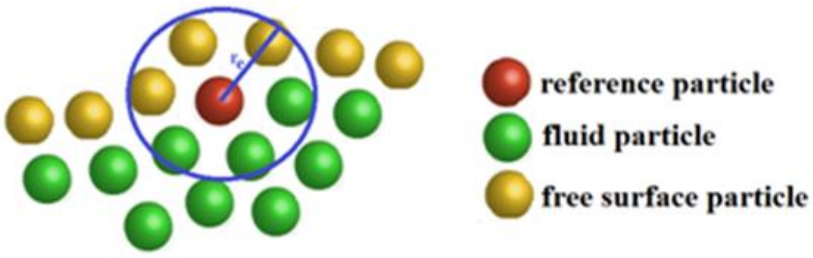

Figure 1. Illustration of radius of interaction which represents region of interaction around a particle

At the position of *i*-particle, the density–proportional to that of the fluid–can be approximated by

$$n_i = \sum_{j \neq i} w\left(|\vec{r}_j - \vec{r}_i|\right) \quad (2)$$

where $\vec{r}_i$ and $\vec{r}_j$ are the position of the *i*-particle and the *j*-particle respectively. Gradient, divergence, and Laplacian of a physical quantity, are approximated as follows

$$\langle \vec{\nabla}\phi \rangle_i = \frac{d}{n^0} \sum_{j \neq i} \frac{\phi_j - \hat{\phi}_i}{|\vec{r}_j - \vec{r}_i|^2} (\vec{r}_j - \vec{r}_i) w\left(|\vec{r}_j - \vec{r}_i|\right) \quad (3)$$

$$\langle \vec{\nabla} \cdot \vec{\varphi} \rangle_i = \frac{d}{n^0} \sum_{j \neq i} \frac{(\vec{\varphi}_j - \vec{\varphi}_i)(\vec{r}_j - \vec{r}_i)}{|\vec{r}_j - \vec{r}_i|^2} w\left(|\vec{r}_j - \vec{r}_i|\right) \quad (4)$$

Computational and Experimental Research in Materials and Renewable Energy (CERiMRE)
Volume 8, Issue 1, page 1-18
eISSN : 2747-173X

Submitted : April 24, 2025
Accepted : May 19, 2025
Online : May 31, 2025
DOI : 10.19184/cerimre.v8i1.53687

$$\langle \nabla^2 \phi \rangle_i = \frac{2d}{\lambda n^0} \sum_{j \neq i} (\phi_j - \phi_i) w(|\vec{r}_j - \vec{r}_i|) \quad (5)$$

Here, d is the number of spatial dimensions, n^0 is the initial particle number density, ϕ_i and ϕ_j are the scalar quantities of the i-particle at $\vec{r}_i$, and the j-particle at $\vec{r}_i$ respectively, $\hat{\phi}_i$ is the lowest value of the scalar quantity in the effective radius of the *i*-target particle, $\vec{\varphi}_i$ and $\vec{\varphi}_j$ are the vectors of the i-particle at $\vec{r}_i$, and the j-particle at $\vec{r}_j$, respectively, and λ is the parameter for constructing the Laplacian model. The formula for calculating λ is given by

$$\lambda = \frac{\sum_{j \neq i} w(|\vec{r}_j - \vec{r}_i|) |\vec{r}_j - \vec{r}_i|^2}{\sum_{j \neq i} w(|\vec{r}_j - \vec{r}_i|)} \cong \frac{\int_V w(r) r^2 dV}{\int_V w(r) dV} \quad (6)$$

The momentum equation, the Navier-Stokes equation, and energy equation, are the governing equations and they are given–respectively as the following

$$\frac{D\rho}{Dt} = 0 \quad (7)$$

$$\frac{Du}{Dt} = -\frac{1}{\rho} \nabla P + \frac{\mu}{\rho} \nabla^2 \vec{u} + \vec{g} \quad (8)$$

$$\frac{\partial T}{\partial t} = \frac{k}{\rho c_p} \nabla^2 T + \dot{q}_v \quad (9)$$

where ρ, t, $\vec{u}$, ∇, P, μ, $\vec{g}$, T, k, c_p, and $\dot{q}_v$ represent the density of the fluid, time, velocity vector, gradient, pressure, dynamic viscosity, acceleration, temperature, thermal conductivity, heat capacity, and heat flux, respectively (as described in [8], [9], [26]).

Numerical Method

In this study, numerical solutions were obtained by combining two computational techniques: the Finite Difference Method with an explicit scheme for handling the viscosity term, and the Crank–Nicholson Method—an efficient implicit approach—for solving the Poisson equation. This hybrid strategy ensured both stability and accuracy in simulating fluid behavior. A detail explanation of two methods can be found in this [27]. The calculation process was commenced by determining the viscous term using [8], [9], [26]

$$\vec{u}_k^* = \vec{u}_i^k + v\Delta t \frac{2d}{\lambda n^0} \times \sum_{j \neq i} (\vec{u}_j^* - \vec{u}_i^*) w(|\vec{u}_j^k - \vec{u}_i^k|) \quad (10)$$

where Δt is the time interval used, superscript $*$ is the temporary value, and superscript k is the previous value. Subsequently, the new temporary velocity $\vec{u}^{**}$ and position of a particle $\vec{r}^{**}$ were determined using the following formula

$$\vec{u}^{**} = \vec{u}^* + \Delta t\, \vec{g} \quad (11)$$

$$\vec{r}^{**} = \vec{r}^k + \Delta t\, \vec{u}^{**} \quad (12)$$

Computational and Experimental Research in Materials and Renewable Energy (CERiMRE)
Volume 8, Issue 1, page 1-18
eISSN : 2747-173X

Submitted : April 24, 2025
Accepted : May 19, 2025
Online : May 31, 2025
DOI : 10.19184/cerimre.v8i1.53687

The next step was to calculate the pressure term in Eq. (8) by solving the Poisson equation, i.e.

$$\frac{1}{\rho^0}\nabla^2 P = \frac{1-\beta}{\Delta t^2}\frac{n^* - 2n^k + n^{k-1}}{n^0} + \frac{\beta-\gamma}{\Delta t^2}\frac{n^* - n^k}{n^0} + \frac{\gamma}{\Delta t^2}\frac{n^* - n^0}{n^0} \tag{13}$$

$$\left(-\frac{1}{\rho^0}\nabla^2 P\right)_i = -\frac{1}{\rho^0}\frac{d}{n^0}\sum_{j\neq i}\left[\frac{P_j - \hat{P}_i}{\left|\vec{r}_j - \vec{r}_i\right|^2}\left(\vec{r}_j - \vec{r}_i\right)w\left(\left|\vec{r}_j - \vec{r}_i\right|, r_e\right)\right] \tag{14}$$

Then, following [8], [9], [26], the particle velocity and position corrections can be computed as

$$\vec{u}^{k+1} = \vec{u}^{**} + \Delta t\left(-\frac{1}{\rho^0}\nabla P\right) \tag{15}$$

$$\vec{r}^{k+1} = \vec{r}^{**} + (\Delta t)^2\left(-\frac{1}{\rho^0}\nabla P\right) \tag{16}$$

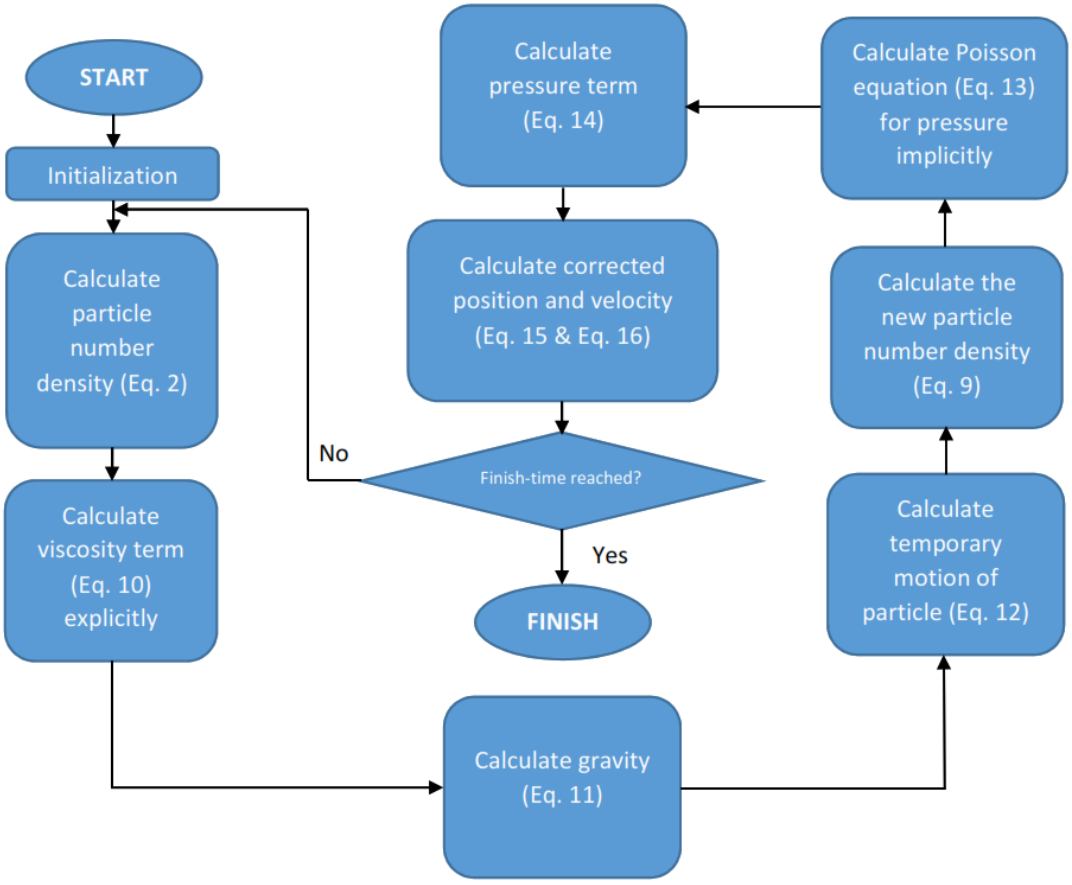

Figure 2. The current calculation process of the MPS method

Computational and Experimental Research in Materials and Renewable Energy (CERiMRE)
Volume 8, Issue 1, page 1-18
eISSN : 2747-173X

Submitted : April 24, 2025
Accepted : May 19, 2025
Online : May 31, 2025
DOI : 10.19184/cerimre.v8i1.53687

Figure 2 shows the MPS simulation algorithm. First, the number density was calculated, and then the location and velocity were initialized. Calculations were then performed for the viscosity, gravity, and pressure. The discharge coefficient of liquid C_d is calculated using the following formula [28], [29], [30], [31]

$$C_d = 2\left(\frac{D}{d}\right)^2 \frac{\sqrt{H}-\sqrt{h}}{t_{disch}\sqrt{2g}} \tag{17}$$

where D is the diameter of the tank, d is the diameter of the exhaust hole, H is the initial surface level, h is the surface level after t second, and t_{disch} is discharge time. The Reynolds number Re can be calculated using

$$Re = \frac{u\,D}{\upsilon} \tag{18}$$

where u is the velocity of liquid and υ is the kinematic viscosity.

Table 1. The parameters of the liquids [19], [32].

Liquids	$T_{simulation}$ (K)	Density (kg m^{-3})	Kinematic viscosity (m^2 s^{-1})
light water	298	1.00×10^3	1.00×10^{-6}
FLiBe	1500	1.681×10^3	8.43479×10^{-7}
FLiNaK	1500	1.643×10^3	3.92429×10^{-7}

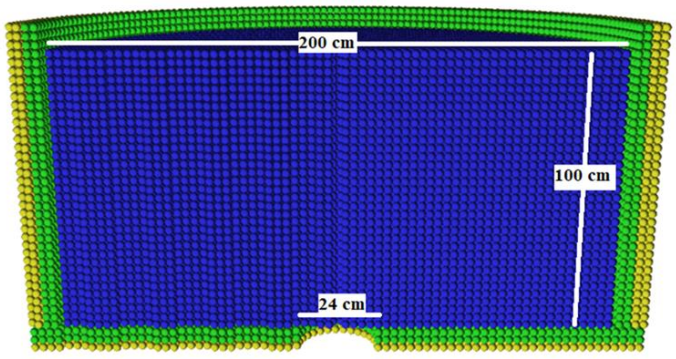

Figure 3. The schematic of simulation

Computational and Experimental Research in Materials and Renewable Energy (CERiMRE)
Volume 8, Issue 1, page 1-18
eISSN : 2747-173X

Submitted : April 24, 2025
Accepted : May 19, 2025
Online : May 31, 2025
DOI : 10.19184/cerimre.v8i1.53687

Simulation

The aim of this study is to examine the characteristics of the liquid within the tank during the discharge procedure. **Figure 3** illustrates the experimental configuration employed in prior investigations, which corresponds to the procedures conducted by Rechiman et al. [23]. The density and the kinematic viscosity for each liquid can be seen in **Table 1** as explained in [19] and [32]. In this study, we considered the discharge of three different liquids, which are light water, FLiBe, and FLiNaK. Each of them were placed in a tank where the geometry is shown in **Figure 3**. After that, the liquid experienced the free fall via the hole in the bottom of the tank. Simulation was performed using the adopted source-code from [15], [18], [19]. The MPS simulation was conducted in 3D configuration for 25 seconds (25 s) with 166,215 particles for each liquid. The image processing technique was utilized to evaluate the outcome at a particular time. In this study, the surface level of the liquid inside the tank, velocity of discharge, pressure distribution, discharge rate, discharge coefficient, and Reynolds number were analyzed to study the behavior of the liquid inside the tank during discharge process. In this simulation, the temperature of the liquid was neglected. This means that the heat transfer process was not included in the calculation.

Result

This study observed the simulation of drain tank. First step, a sensitivity analysis was performed to observe its impact on the output or results of simulations. The obtained results were compared with those of Rechiman et al. [23]. **Figure 4** shows the surface level of the light water inside the tank over a 25-second period every 5 s. The amount of light water in the tank has almost run out after 25 s. It is evident that the surface level of light water decreased over time.

In addition, **Figure 5** shows the velocity of liquid discharge as a function of pressure where the velocity increases as the pressure increases. For light water, when the hydrostatic pressure was 9216.9 Pa, the velocity of the light water was 3.77 m/s. When the pressure decreased to 1074.3 Pa, the velocity of liquid was 2.39 m/s. For FLiBe, when the hydrostatic pressure was 14298 Pa, its velocity was 3.99 m/s. The liquid had a velocity of 2.16 m/s when the pressure dropped to 1577.9 Pa. In the case of FLiNaK, the velocity of liquid was 3.93 m/s when the hydrostatic pressure was 16699 Pa. It dropped to 1.89 m/s when the hydrostatic pressure dropped to 1108.7 Pa. This means that the lower the pressure, the lower the velocity of liquid.

Figure 6 shows the pressure distribution of each liquid at the bottom of the tank throughout a certain time interval, measured in Pascal (Pa). Based on this figure, it reasonable to assume that the pressure at the bottom of the tank decreased with time.

Computational and Experimental Research in Materials and Renewable Energy (CERiMRE)
Volume 8, Issue 1, page 1-18
eISSN : 2747-173X

Submitted : April 24, 2025
Accepted : May 19, 2025
Online : May 31, 2025
DOI : 10.19184/cerimre.v8i1.53687

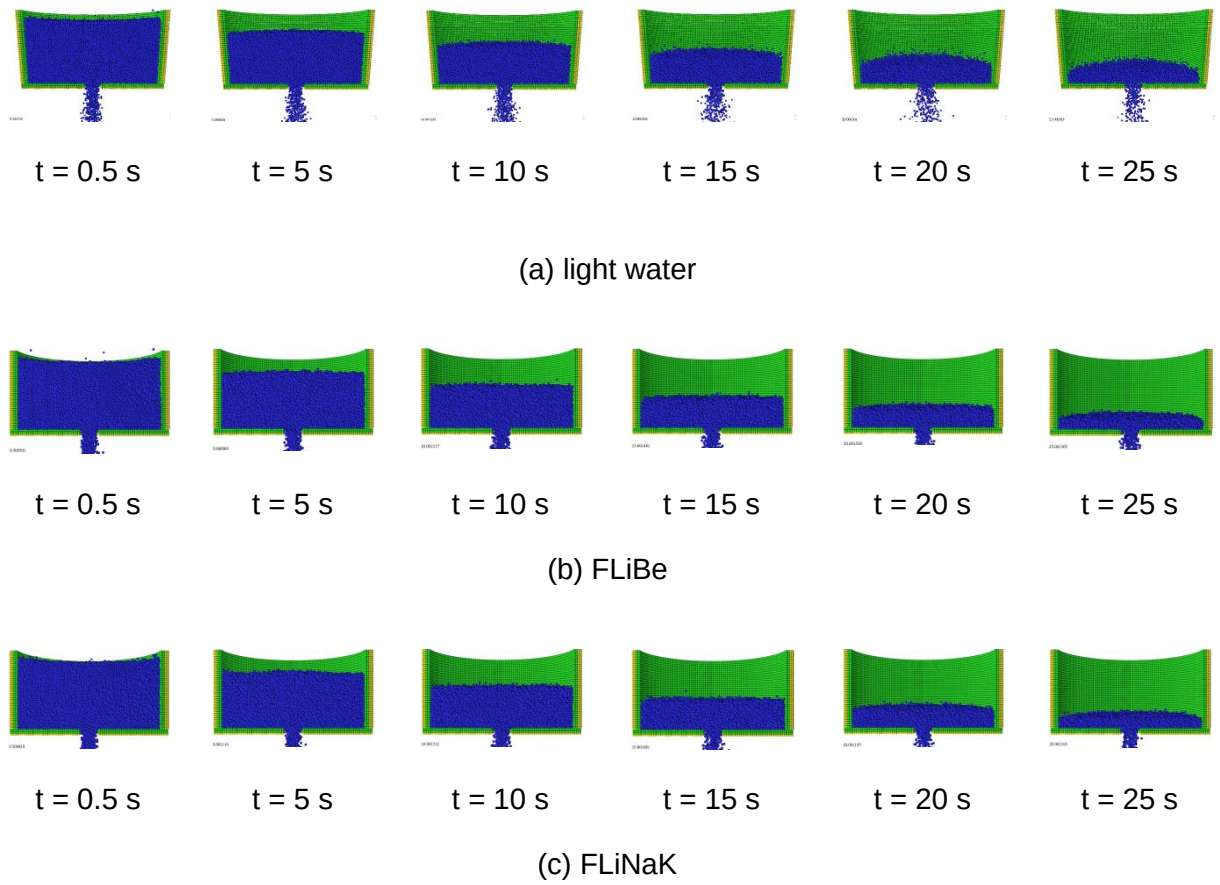

Figure 4. The surface level of each liquid inside the tank with time.

Figure 7 provides information about the effect of surface level on hydrostatic pressure. The initial hydrostatic pressure for light water particles was 8954 Pa when the liquid level was at 0.95 m. As the liquid level dropped to 0.21 m, the hydrostatic pressure decreased to 2714 Pa. The FLiBe particles experienced an initial hydrostatic pressure of 13549 Pa when the liquid height was 0.95 m. This pressure decreased substantially to 1741 Pa when the liquid level dropped to 0.16 m. For the FLiNaK particles, the hydrostatic pressure started at 15510 Pa when the liquid height was 0.95 m, and decreased to 1108 Pa as the liquid level decreased to 0.15 m. It can be seen that the higher the surface level, the greater the hydrostatic pressure of the liquid.

Figure 8 provides important insight into the fluctuating volumes of various liquids by displaying the changes in the liquid volume within the tank over time. This figure shows that at the beginning, the initial volume of each liquid was 3.14 m^3, which was uniform. The amount of liquid showed clear variations as the timer approaches the 25-second. The volume of light water dropped to 0.66 m^3. Concurrently, FLiBe and FLiNaK levels decreased as well, arriving at 0.49 m^3 and 0.47 m^3, respectively.

Computational and Experimental Research in Materials and Renewable Energy (CERiMRE)
Volume 8, Issue 1, page 1-18
eISSN : 2747-173X

Submitted : April 24, 2025
Accepted : May 19, 2025
Online : May 31, 2025
DOI : 10.19184/cerimre.v8i1.53687

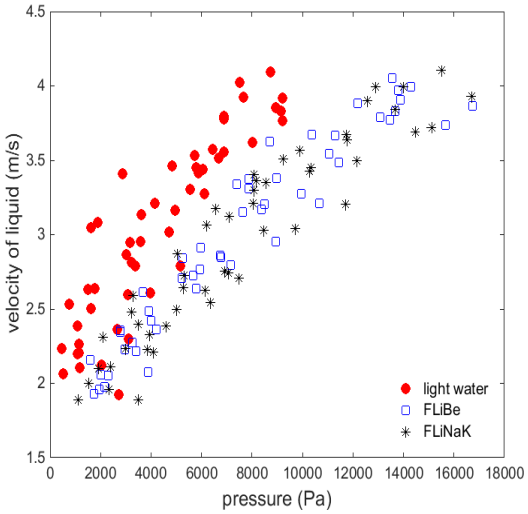

Figure 5. The velocity of discharge as a function of pressure.

A visual representation of the discharge coefficient at various liquid levels is shown in **Figure 9**, which offers important details regarding the functioning of the system with various liquids. The obtained data showed that light water, FLiBe, and FLiNaK at different liquid levels had different discharge coefficients. For light water, the discharge coefficients were between 0.1729 and 1.6651. For FLiBe, the discharge coefficients varied between 0.1052 and 1.5043. The discharge coefficients for FLiNaK were from 0.2345 to 1.5654. It indicates that the discharge coefficients of liquids were between 0.6 and 0.8. In addition, the discharge rate of liquids were between 0.1 m^3/s and 0.15 m^3/s.

In addition, **Figure 10** provides valuable information on the time-based patterns of the liquid discharge by showing the rate of liquid release from the exhaust hole each second. The data demonstrated clear discharge patterns for light water, FLiBe, and FLiNaK within 25 s. The first discharge of light water at t = 0.5 s was recorded as 0.33 m^3/s, and then it remained stable at around 0.12 m^3/s from t = 5 s to t = 25 s. A similar result was also found for FLiBe, where the flow rate of FLiBe started at 0.30 m^3/s and remained constant at a rate of 0.12 m^3/s from t = 5 s to t = 25 s. Similarly, the release of FLiNaK at t = 0.5 s was measured at a rate of 0.31 m^3/s, and it remained consistent at around 0.12 m^3/s after 25 s.

Computational and Experimental Research in Materials and Renewable Energy (CERiMRE)
Volume 8, Issue 1, page 1-18
eISSN : 2747-173X

Submitted : April 24, 2025
Accepted : May 19, 2025
Online : May 31, 2025
DOI : 10.19184/cerimre.v8i1.53687

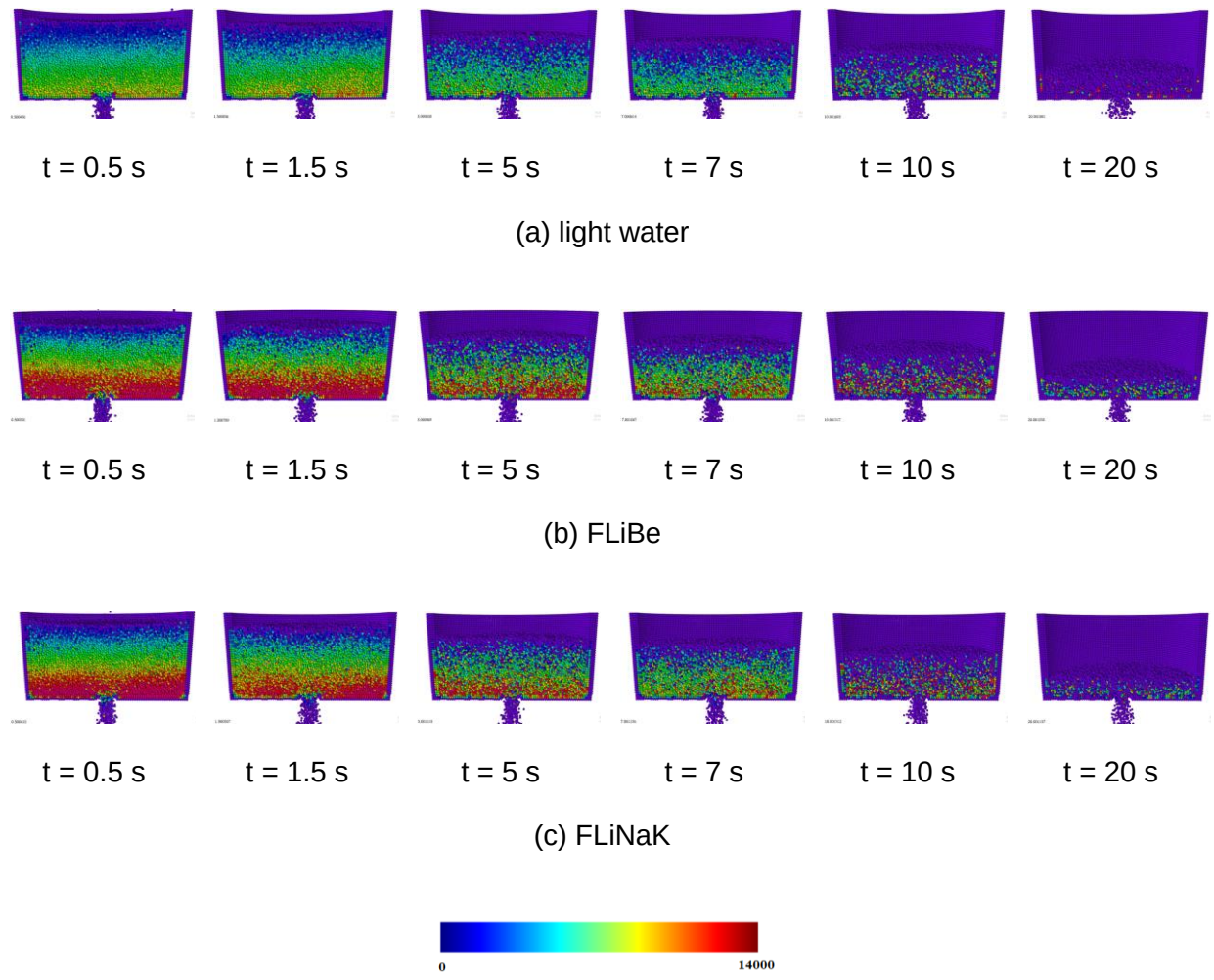

Figure 6. The distribution of pressure within the tank for each liquid.

Figure 11 presents a detailed representation of the variations in Reynolds numbers over time in an exhaust system, revealing dynamic liquid behavior. The Reynolds number for light water varied between 9×10^5 and 0.86×10^5, the Reynolds number of FLiBe ranged from 1.17×10^6 to 0.17×10^6, while the Reynolds number of FLiNaK varied from 1.89×10^6 to 0.34×10^6. These results indicates a wide range of liquid flow dynamics. The Reynolds number of FLiNaK were the greatest among the three liquids.

Computational and Experimental Research in Materials and Renewable Energy (CERiMRE)
Volume 8, Issue 1, page 1-18
eISSN : 2747-173X

Submitted : April 24, 2025
Accepted : May 19, 2025
Online : May 31, 2025
DOI : 10.19184/cerimre.v8i1.53687

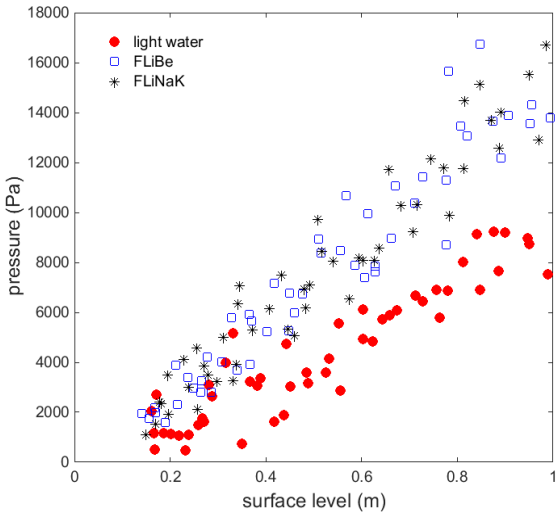

Figure 7. Hydrostatic pressure of the bottom of the tank for each liquid as a function of surface level.

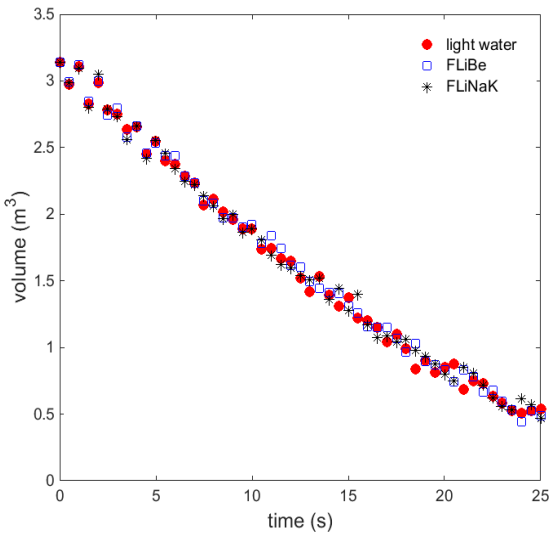

Figure 8. The volume of liquid inside the tank as a function of time.

Computational and Experimental Research in Materials and Renewable Energy (CERiMRE)
Volume 8, Issue 1, page 1-18
eISSN : 2747-173X

Submitted : April 24, 2025
Accepted : May 19, 2025
Online : May 31, 2025
DOI : 10.19184/cerimre.v8i1.53687

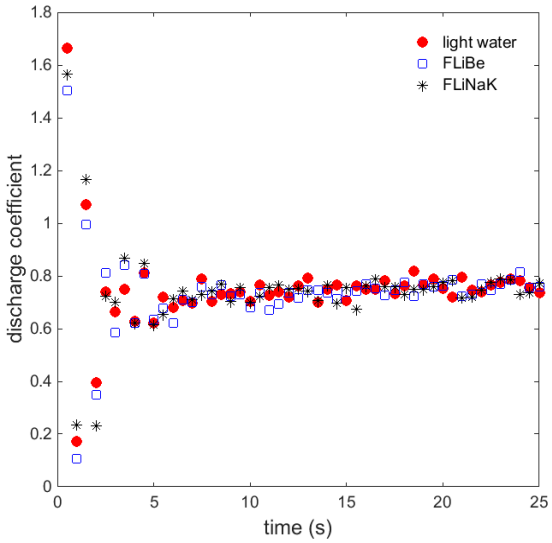

Figure 9. Discharge coefficient as a function of time.

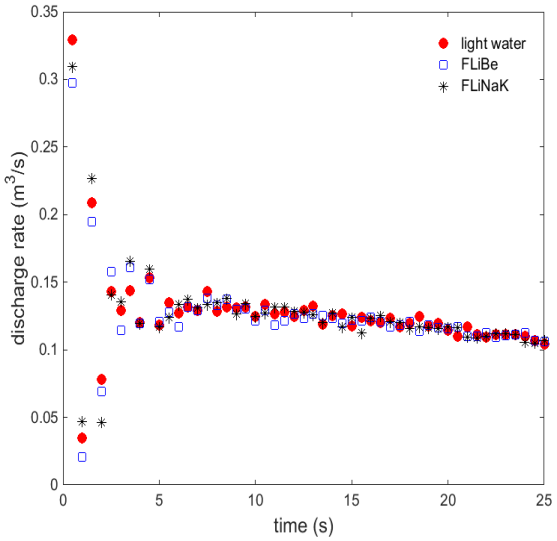

Figure 10. Discharge rate as a function of time.

Computational and Experimental Research in Materials and Renewable Energy (CERiMRE)
Volume 8, Issue 1, page 1-18
eISSN : 2747-173X

Submitted : April 24, 2025
Accepted : May 19, 2025
Online : May 31, 2025
DOI : 10.19184/cerimre.v8i1.53687

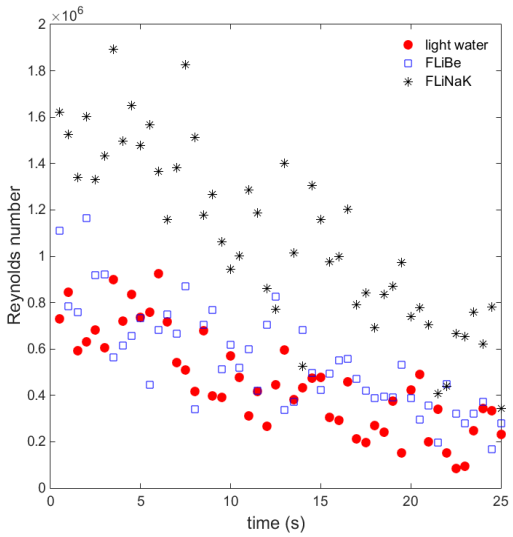

Figure 11. Reynolds number as a function of time

Discussion

For light water, FLiBe, and FLiNaK, **Figure 5** shows that the lower the hydrostatic pressure, the lower the velocity of liquid. In addition, velocity of light water was the greatest among the three fluids considered in this study. This means that the density and kinematic viscosity of the each liquid plays significant role in fluid discharge from the tank. However, it needs further investigations especially the physical parameter that affects the discharge process.

As shown in **Figure 6**, the results demonstrate a decrease for the hydrostatic pressure experienced by particles at the bottom of the tank. From this figure, it can be seen that light water had the lowest hydrostatic pressure among the three liquids while FLiBe and FLiNaK had a similar pattern. In can be inferred that the density of the liquid affected the hydrostatic pressure. The greater the density of the liquid, the greater the hydrostatic pressure.

From **Figure 7**, it can be observed that the hydrostatic pressure experienced by the particles at the bottom of the tank is proportional to the drop in the liquid level in the tank. It is clearly seen that the pressure of light water was the lowest among the three liquids. This implies that the density of the liquid affects the hydrostatic pressure at the bottom of the tank. A comprehensive understanding of fluid mechanics in an experimental context is made possible by the important information provided by the relationship between hydrostatic pressure and liquid level during the discharge process.

Figure 8 highlights the change in liquid volumes inside the tank, as all three liquids exhibited a significant drop in volume throughout the observation. The observed fluctuations offer useful insights into the dynamics of liquids under experimental settings, elucidating the temporal changes in the volumes of light water, FLiBe, and FLiNaK within the specified framework.

Computational and Experimental Research in Materials and Renewable Energy (CERiMRE)
Volume 8, Issue 1, page 1-18
eISSN : 2747-173X

Submitted : April 24, 2025
Accepted : May 19, 2025
Online : May 31, 2025
DOI : 10.19184/cerimre.v8i1.53687

Figure 9 provides a clear understanding of the discharge characteristics of each liquid under investigation, illustrating the differences in the discharge coefficients at different liquid levels. Subtle differences in the discharge performances of light water, FLiBe, and FLiNaK were suggested by the measured ranges. An important method to assess the efficiency and consistency of the liquid discharge process is to determine the discharge coefficient of the liquid levels. This aids in system performance optimization and understanding under various conditions. This information is helpful for comprehending and examining the dynamics of discharge in the exhaust hole throughout the indicated time interval.

Figure 10 emphasizes the discharge rate of each liquid, revealing clear temporal patterns in the liquid discharge. The discharge rate can be utilized to predict how long it takes to empty the tank. This also provides information on how long the heat can be removed from the reactor core during a severe accident, preventing overheating, and maintaining a safe temperature. The pump and piping systems within the MSR must be designed to accommodate specified flow rates. The selection and sizing of pumps as well as the overall layout of the fluid transport system depend on the desired flow characteristics.

In **Figure 11**, the large variation implies transitions between turbulent and laminar flow patterns and demonstrates a dynamic evolution in the flow state. The fluid dynamics of the exhaust system can be better understood by examining fluctuations in the Reynolds number. A transition between turbulent and laminar states may have occurred because the broad spectrum revealed significant variation in the characteristics of the liquid flow. Maximizing the efficiency of the system's operation and design requires a thorough understanding of these variances. The range of data highlights the importance of considering the Reynolds numbers for system optimization by pointing to complex variations in the flow conditions over time. An important understanding of the fluid dynamics of light water, FLiBe, and FLiNaK in exhaust systems is provided by this thorough analysis of Reynolds numbers. For engineers and researchers, it is an indispensable tool that helps them create and run systems that are specifically made to fit the unique characteristics of each part.

Conclusions

The discharge process was simulated using three different liquids, which are light water, FLiBe, and FLiNaK. This study was performed to investigate the behavior of liquid during the discharge process of Molten Salt Reactor. Simulation was performed for 25 s by using the Moving Particle Semi-Implicit method. The study compares the behavior of three different liquids—light water, FLiBe, and FLiNaK—during discharge under varying hydrostatic pressures. When the tank was filled with light water, the flow velocity started at 3.77 m/s under a pressure of 9216.9 Pa and decreased to 2.39 m/s as the pressure dropped to 1074.3 Pa. For FLiBe, the velocity was 3.99 m/s at 14298 Pa and reduced to 2.16 m/s at 1577.9 Pa. Similarly, FLiNaK showed a velocity of 3.93 m/s at 16699 Pa, which declined to 1.89 m/s at 1108.7 Pa. Initial hydrostatic pressures at a liquid height of 0.95 m were 8954 Pa for light water, 13549 Pa for FLiBe, and 15510 Pa for FLiNaK. As the liquid levels dropped to approximately 0.15–0.21 m, the corresponding pressures decreased significantly to 2714 Pa, 1741 Pa, and 1108 Pa, respectively. Initially, each liquid had a volume of 3.14 m^3. After 25 seconds, the volumes declined to 0.66 m^3 for light water, 0.49 m^3 for FLiBe, and 0.47 m^3 for FLiNaK, indicating substantial discharge. The discharge coefficients ranged between 0.1729 and 1.6651 for light water, 0.1052 to 1.5043 for FLiBe, and 0.2345 to 1.5654 for FLiNaK, with most values clustering between 0.6 and 0.8.

Computational and Experimental Research in Materials and Renewable Energy (CERiMRE)
Volume 8, Issue 1, page 1-18
eISSN : 2747-173X

Submitted : April 24, 2025
Accepted : May 19, 2025
Online : May 31, 2025
DOI : 10.19184/cerimre.v8i1.53687

Discharge rates across all liquids generally ranged from 0.1 to 0.15 m^3/s. Each liquid initially discharged rapidly—about 0.30–0.33 m^3/s at t = 0.5 s—and stabilized at approximately 0.12 m^3/s by t = 5 s through t = 25 s. In terms of flow regime, Reynolds numbers indicated turbulent flow for all fluids: light water ranged from 9×10^5 to 0.86×10^5, FLiBe from 1.17×10^6 to 0.17×10^6, and FLiNaK from 1.89×10^6 to 0.34×10^6. The obtained results showed that the patterns observed in the decreasing liquid levels were similar, although the liquids differed in density and viscosity kinematics. Indicating similar dynamic responses, the three liquids showed comparable patterns over the observed time frame. The velocity, hydrostatic pressure, and Reynolds number of liquids decreased over time. The process of heat transfer was not the main focus of this investigation. It would be fascinating to take into account the heat transfer when performing calculations in the future.

Acknowledgements

The PPMI ITB Bandung program provided all funding for this project. The fundamental MPS code script for liquids was facilitated by Professor S. Koshizuka, Professor M. Sakai, and Dr. K. Shibata from the University of Tokyo. The author wishes to express gratitude for this kind of help.

References

[1] H. Peng, M. Shen, Y. Zuo, H. Fu, and L. Xie, “Chemical and electrochemical studies on the solubility of UO2 in molten FLINAK with ZrF4 additive,” *Journal of Nuclear Materials*, vol. 510, pp. 256–264, 2018, doi: 10.1016/j.jnucmat.2018.08.013.

[2] C. N. A. C. Z. Bahri, W. M. Al-Areqi, M. I. F. M. Ruf, and A. A. Majid, “Characteristic of molten fluoride salt system LiF-BeF2 (Flibe) and LiF-NaF-KF (flinak) as coolant and fuel carrier in molten salt reactor (MSR),” *AIP Conference Proceedings*, vol. 1799, pp. 1–8, 2017, doi: 10.1063/1.4972932.

[3] P. R. Rubiolo, M. T. Retamales, V. Ghetta, and J. Giraud, “High temperature thermal hydraulics modeling of a molten salt: application to a molten salt fast reactor (MSFR),” *ESAIM: Proceedings and Surveys*, vol. 58, no. December 2017, pp. 98–117, 2019.

[4] O. Ashraf, A. D. Smirnov, and G. V. Tikhomirov, “Nuclear fuel optimization for molten salt fast reactor,” *Journal of Physics: Conference Series*, vol. 1133, no. 1, 2018, doi: 10.1088/1742-6596/1133/1/012026.

[5] R. R. Romatoski and L. W. Hu, “Fluoride salt coolant properties for nuclear reactor applications: A review,” *Annals of Nuclear Energy*, vol. 109, pp. 635–647, 2017, doi: 10.1016/j.anucene.2017.05.036.

[6] R. Freile and M. Kimber, “Influence of molten salt-(FLiNaK) thermophysical properties on a heated tube using CFD RANS turbulence modeling of an experimental testbed,” *EPJ Nuclear Sci. Technol.*, vol. 5, no. 16, pp. 1–13, 2019, doi: https://doi.org/10.1051/epjn/2019027.

Computational and Experimental Research in Materials and Renewable Energy (CERiMRE)
Volume 8, Issue 1, page 1-18
eISSN : 2747-173X

Submitted : April 24, 2025
Accepted : May 19, 2025
Online : May 31, 2025
DOI : 10.19184/cerimre.v8i1.53687

[7] C. Fiorina, A. Cammi, L. Luzzi, K. Mikityuk, H. Ninokata, and M. E. Ricotti, "Thermal-hydraulics of internally heated molten salts and application to the Molten Salt Fast Reactor Thermal-hydraulics of internally heated molten salts and application to the Molten Salt Fast Reactor," *Journal of Physics: Conference Series*, vol. 501, p. 012030, 2014, doi: 10.1088/1742-6596/501/1/012030.

[8] S. Koshizuka and Y. Oka, "Moving-Particle Semi-Implicit Method for Fragmentation of Incompressible Fluid," *Nuclear Science and Engineering*, vol. 123, pp. 421–434, 1996, doi: 10.13182/NSE96-A24205.

[9] S. Koshizuka, S. Kazuya, K. Masahiro, and M. Takuya, *Moving Particle Semi-implicit Method - A Meshfree Particle Method for Fluid Dynamics*. Academic Press, 2018.

[10] S. Koshizuka, A. Nobe, and Y. Oka, "Numerical analysis of breaking waves using the Moving Particle Semi-Implicit method," *International Journal for Numerical Methods in Fluids*, vol. 26, pp. 751–769, 1998.

[11] G. Duan, A. Yamaji, and M. Sakai, "A multiphase MPS method coupling fluid–solid interaction/phase-change models with application to debris remelting in reactor lower plenum," *Annals of Nuclear Energy*, vol. 166, p. 108697, 2022, doi: 10.1016/j.anucene.2021.108697.

[12] T. Kawahara and Y. Oka, "Ex-vessel molten core solidification behavior by moving particle semi-implicit method," *Journal of Nuclear Science and Technology*, vol. 49, no. 12, pp. 1156–1164, 2012.

[13] Jubaidah, G. Duan, A. Yamaji, C. Journeau, L. Buffe, and J. F. Haquet, "Investigation on corium spreading over ceramic and concrete substrates in VULCANO VE-U7 experiment with moving particle semi-implicit method," *Annals of Nuclear Energy*, vol. 141, p. 107266, 2020, doi: 10.1016/j.anucene.2019.107266.

[14] M. Ilham, Y. Yulianto, and A. P. A. Mustari, "Simulation on Relocation of Non-Compressed Fluid Flow using Moving Particle Semi-Implicit (MPS) Method," *IOP Conference Series: Materials Science and Engineering*, vol. 407, p. 012100, 2018, doi: 10.1088/1757-899X/407/1/012100.

[15] Y. Yulianto and A. P. A. Mustari, "Numerical Study on Relocation Process of Al, Fe, and Pb by Using the Moving Particle Semi-Implicit Method During Severe Accident of Reactor," *International Journal of Technology*, vol. 14, no. 4, pp. 800–810, 2023, doi: 10.14716/ijtech.v14i4.5240.

[16] A. P. A. Mustari and Y. Oka, "Molten uranium eutectic interaction on iron-alloy by MPS method," *Nuclear Engineering and Design*, vol. 278, pp. 387–394, 2014, doi: 10.1016/j.nucengdes.2014.07.028.

Computational and Experimental Research in Materials and Renewable Energy (CERiMRE)
Volume 8, Issue 1, page 1-18
eISSN : 2747-173X

Submitted : April 24, 2025
Accepted : May 19, 2025
Online : May 31, 2025
DOI : 10.19184/cerimre.v8i1.53687

[17] A. P. A. Mustari, Y. Oka, M. Furuya, W. Takeo, and R. Chen, "3D simulation of eutectic interaction of Pb-Sn system using Moving Particle Semi-implicit (MPS) method," *Annals of Nuclear Energy*, vol. 81, pp. 26–33, 2015, doi: 10.1016/j.anucene.2015.03.031.

[18] Y. Yulianto, A. N. Hidayati, A. P. A. Mustari, M. Ilham, and S. Pramuditya, "Moving Particle Semi-implicit (MPS) Utilization in Analyzing the Stratification Behavior of Immiscible Liquid," *IOP Conference Series: Materials Science and Engineering*, vol. 407, p. 012189, 2018, doi: 10.1088/1757-899X/407/1/012189.

[19] Y. Yulianto, A. P. A. Mustari, and A. Baliana, "The Simulation of the Stratification Process of Some Liquid Salts by Using the Moving Particle Semi-Implicit Method," *Journal of Physics: Conference Series*, vol. 2243, p. 012065, 2022, doi: 10.1088/1742-6596/2243/1/012065.

[20] Y. Yulianto, A. P. A. Mustari, M. Ilham, A. N. Hidayati, and S. Hatmanti, "Moving Particle Semi-implicit Method in Simulating Water-Oil Penetration," *Indonesian Journal of Physics*, vol. 30, no. 2, pp. 25–33, 2019.

[21] Y. Yulianto, A. P. A. Mustari, and A. Baliana, "The stratification behavior of reactor materials in the framework of Moving Particle Semi-Implicit," *Indonesian Journal of Nuclear Science and Technology*, vol. 02, no. 02, pp. 59–71, 2021.

[22] Y. Yulianto, "Investigation of hydraulic jump by using the Moving Particle Semi-Implicit method," *Indonesian Journal of Physics*, vol. 34, no. 1, pp. 25–37, 2023.

[23] L. M. Rechiman, M. I. Cantero, and E. A. Dari, "Hydrodynamic transient assessment of a draining tank," *Mecánica Computacional*, vol. 33, pp. 2927–2938, 2014.

[24] A. M. Leandro, F. Heidet, R. Hu, and N. R. Brown, "Thermal hydraulic model of the molten salt reactor experiment with the NEAMS system analysis module," *Annals of Nuclear Energy*, vol. 126, pp. 59–67, 2019, doi: 10.1016/j.anucene.2018.10.060.

[25] K. Kotharu, "System Design and Description of a Molten Salt Loop," Rensselaer Polytechnic Institute, 2021.

[26] S. Koshizuka and Y. Oka, "Mowing Particle Semi-Implicit Method: Fully Lagrangian Analysis of Incompressible Flows," in *European Congress on Computational Methods in Applied Sciences and Engineering*, Barcelona, 2000, pp. 1–16.

[27] S. C. Chapra and R. P. Canale, *Numerical methods for engineers*, Sixth. New York: McGraw-Hill, 2006.

[28] F. M. Sakri, M. S. M. Ali, S. A. Z. S. Salim, and S. Muhamad, "Numerical Simulation of Liquids Draining From a Tank Using OpenFOAM," *IOP Conference Series: Materials*

Computational and Experimental Research in Materials and Renewable Energy (CERiMRE)
Volume 8, Issue 1, page 1-18
eISSN : 2747-173X

Submitted : April 24, 2025
Accepted : May 19, 2025
Online : May 31, 2025
DOI : 10.19184/cerimre.v8i1.53687

Science and Engineering, vol. 226, p. 012152, 2017, doi: 10.1088/1757-899X/226/1/012152.

[29] F. M. Sakri, M. S. M. Ali, and S. A. Zaki, “Benchmark on the Dynamics of Liquid Draining Inside a Tank,” in *The 3rd International Conference on Power, Energy and Mechanical Engineering (ICPEME 2019)*, 2019, pp. 1–6.

[30] C. Rubio *et al.*, “Discharge time of a water tank through orifices,” *International Journal of Civil Engineering and Technology (IJCIET)*, vol. 10, no. 01, pp. 2587–2593, 2019.

[31] S. Wang, M. Massone, A. Rineiski, and E. Merle-Lucotte, “Analytical Investigation of the Draining System for a Molten Salt Fast Reactor,” in *The 11th International Topical Meeting on Nuclear Reactor Thermal Hydraulic, Operation, and Safety*, 2016.

[32] IAEA, *Thermophysical Properties of Materials For Nuclear Engineering: A Tutorial and Collection of Data*. Vienna: IAEA, 2008.